

## **Supplementary information to: Dahl et al. Uranium isotopes distinguish two geochemically distinct stages during the later Cambrian SPICE event**

### **Contents**

- S1. U burial from seawater into carbonates
- S2. Model for the dynamical evolution of seawater chemistry during the event
- S3. Reservoir effect, characteristic time scales, stratigraphic residence time

### **S1. U burial process in anoxic carbonate sediments — pH, speciation, $\delta^{238}\text{U}$**

The upper part of the Mt. Whelan drill core displays abrupt shifts in  $\delta^{238}\text{U}$  decoupled from secular changes in open ocean composition. Our favored explanation is that sulfate reduction exerts important control on U speciation in the sedimentary pore fluids. This idea has not yet been demonstrated by laboratory experiments or field observations, but is founded solely on reasonable theoretical expectations - and matches the observed coincidence between frequent  $\delta^{238}\text{U}$  jumps and intervals without any observable S isotope fractionation ( $\Delta^{34}\text{S}$ ) in the Mt. Whelan #1 drill core.

It is likely that sulfate reduction, by producing both  $\text{HS}^-$  and  $\text{H}^+$ , lowers pH in sulfidic marine carbonate sediments (pH = 7.1-7.6, Romaniello, 2012) relative to both oxic and anoxic/non-sulfidic sediments (pH = 7.4-7.9, Goldberg et al., 2012), thus promoting the conversion of uranyl-tricarbonate complexes to uranyl-phosphate complexes, (Langmuir, 1978) contributing to the observed constant +0.31‰ uranium isotopic offset in sulfidic sediments under oxic waters. Uranium reduction takes place in the sediments, perhaps abiotically with  $\text{HS}^-$  or via sulfate reducing bacteria (Bargar et al., 2013; Hua et al., 2006; Lovley et al., 1993; Tucker et al., 1998), and, U removal occurs below the sediment-water interface from the dissolved U pool in the interstitial waters. Since sulfate reduction typically causes a larger pH change, we speculate that this could explain the apparent binary nature of the isotope shift observed both in the modern and in the Mt. Whelan data.

Alternative hypotheses for the systematic negative  $\delta^{238}\text{U}$  excursion observed in the carbonate-associated uranium include a range of scenarios linked to changes in net isotopic between contemporaneous seawater and sediments in the Georgina Basin. For example, a negative  $\delta^{238}\text{U}$  excursion may result if the depth to the non-reactive zone migrated further into the sediments causing muted isotope fractionation relative overlying seawater. This would conform to a sea level drop, presumably higher  $\text{O}_2$  in the bottom water and a greater  $\text{O}_2$  penetration depth in the sediments (Figure 7). In this scenario, one should expect a systematic positive correlation between  $\delta^{238}\text{U}$  and total organic carbon contents (TOC) in the sediments with the lowest  $\delta^{238}\text{U}$  values (smallest fractionation) linked to greatest  $\text{O}_2$  penetration depth and lowest sedimentary TOC contents. Only sparse TOC data exist for the Mt. Whelan drill core (Saltzman et al. 2011). However, the data shows no correlation between TOC and  $\delta^{238}\text{U}$  (Figure S1). This already contradicts with migration of the reactive zone as a causal mechanism for the negative U isotope excursion. Furthermore, the link between sea level drop and negative  $\delta^{238}\text{U}$  excursion is out of phase by ~50 m (Figure 7). It is also important to note that Holocene drill cores from the Bahamas carbonate platform show no systematic  $\delta^{238}\text{U}$  changes, despite sea level has risen ~30 meter at this time (Lighty et al., 1982; Romaniello, 2012).

Clearly, local uranium isotope fractionation processes warrants a very critical eye. To test whether the systematic trends for  $\delta^{238}\text{U}$  can be ascribed changes in the removal process in the local basin, a comparison is made to other geochemical data, including proxy measures for diagenetic alteration (Mn/Sr) and for dolomitization (Mg/Ca). These data sets are uncorrelated to the negative U isotope excursion (Figure S1). Thus, the systematic negative  $\delta^{238}\text{U}$  excursion at the onset of the SPICE event represents a true signal of changing seawater composition.

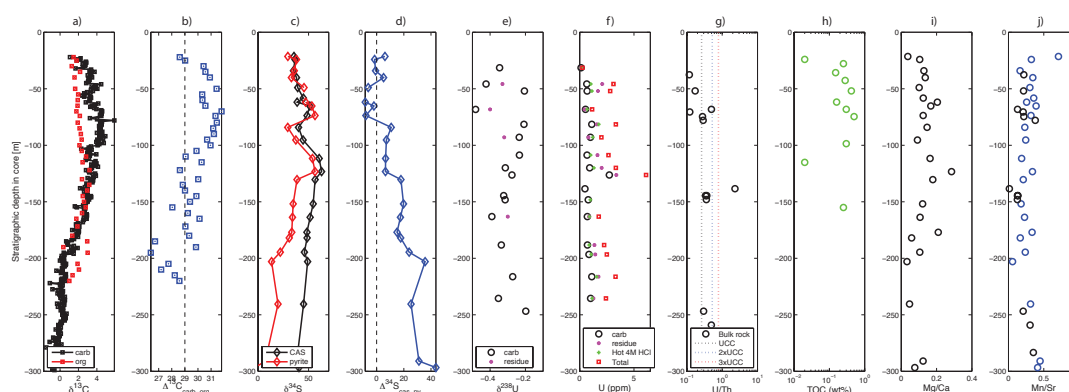


Figure S1. Summary of supporting data from the Mt. Whelan #1 drill core. a)  $\delta^{13}\text{C}$  of carbonate (black) and organic matter (red) (Saltzman et al., 2011), b)  $\Delta^{13}\text{C} = \delta^{13}\text{C}_{\text{carbonate}} - \delta^{13}\text{C}_{\text{organic}}$  (Saltzman et al., 2011), c)  $\delta^{34}\text{S}$  of carbonate-associated sulfate (black) and pyrite (red) (Gill et al., 2011), d)  $\Delta^{34}\text{S} = \delta^{34}\text{S}_{\text{CAS}} - \delta^{34}\text{S}_{\text{pyrite}}$  (Gill et al., 2011), e)  $\delta^{238}\text{U}$  of carbonate-associated uranium (-0.7‰ outlier at 138.5m is not shown, Table S1), f) carbonate-associated U (black,  $\bullet$ ), U leachable in hot 4M HCl (green,  $+$ ), residual U unreactive in HCl (purple,  $\blacksquare$ ) and total sedimentary U contents (red,  $\square$ ), g) U/Th ratios in carbonate leaches compared to average upper continental crust (semi-logarithmic scale), h) sedimentary TOC contents (Saltzman et al., 2011), i) Mg/Ca (Gill et al., 2011), and j) Mn/Sr (Gill et al., 2011; this work). The lack of correlation between  $\delta^{238}\text{U}$  and Mg/Ca indicates that dolomitization did not significantly skew their uranium isotope values. Mn/Sr is commonly used as an indicator for diagenetic alteration. The lack of correlation between  $\delta^{238}\text{U}$  and Mn/Sr indicate that diagenesis did not significantly affect the uranium isotope values.

### Table S1: U contents in Mt Whelan #1 sediments.

(TableS1\_SupplementaryData.xlsx)

## S2. Model: Dynamical evolution of seawater chemistry during the anoxic oceanic event

### Simple ocean model

The ocean model presented here is a one-compartment box model that calculates the inventories of C, S and U and their isotope compositions in response to changes in fluxes into/out of the ocean. The following two equations describes the dynamic evolution of seawater composition for each of the elemental cycles:

$$\text{(eq. S1, eq. 1)} \quad dM/dt = J_{in} - \sum_i J_{out,i}$$

$$\text{(eq. S2, eq. 2)} \quad d(M\delta)/dt = \delta_{in} J_{in} - \sum_i (\delta - \Delta_i) J_{out,i}$$

Here,  $M$  and  $\delta$  are the oceanic inventory and isotope composition for each element, respectively. A total of six equations are written for carbon, sulfur and uranium. The major marine sinks ( $J_{out,i}$ ) are listed in Table 1 and subscript “i” represents each sink in the equations. The sink flux is a function of a distinct removal rate ( $a_i$ ) that is a function of the sedimentation rate, areal extent of the sink, and mass-specific removal efficiency at a given concentration in seawater. The response to changing seawater concentrations for each sink is given by the following equation.

$$\text{(eq. S3)} \quad J_{out,i} = b_i M^{a_i}$$

The boundary conditions for the model are the oceanic source fluxes and oceanic inventories thought to be representative of the Cambrian ocean and are listed in Table S2. Finally, all net isotope fractionation factors ( $D_i$ ) are first assumed constant at modern values (Table S3), but later we relax this assumption.

The model was first calibrated at the modern ocean elemental and isotopic compositions Table S2, and was later adjusted to Cambrian steady state conditions. The SPICE burial episode is modeled as a perturbation to this Cambrian ocean state. The steady-state model approximation is acceptable so long as the perturbations are significantly larger than the adjustments necessary to initialize the system to steady state.

**Table S2: Summary of steady state inventories, fluxes and isotope compositions explored in the Cambrian ocean models (listed in Table S4 and S5) and the values used for calibration to the modern ocean. The model values that yield the composition of the modern ocean are shown in column 2 and 3.**

	<b>Modern model (calibration)</b>	<b>Typical modern values<sup>fi</sup></b>	<b>Reference</b>	<b>Cambrian model range normalized to modern calibration</b>
<b>Fluxes [moles/yr]</b>				
Oceanic C input	$26 \cdot 10^{12}$	$25 \cdot 10^{12}$	(Gill et al., 2011)	0.25-1.0
Oceanic S input	$1.8 \cdot 10^{12}$	$1.5 \cdot 10^{12}$	(Gill et al., 2011)	0.40-1.0
Oceanic U input	$5.6 \cdot 10^7$	$5.3 \cdot 10^7$	(Dunk et al., 2002)	0.25-1.0
<b>Isotope compositions</b>				
$\delta^{13}\text{C}$ marine input	$-5.8\text{‰}^{\Omega}$	-6 to -4‰	(Gill et al., 2011)	-6.2‰
$\delta^{34}\text{S}$ marine input	$2.0\text{‰}^{\Omega}$	0-8‰	(Gill et al., 2011)	0‰
$\delta^{238}\text{U}$ marine input	$-0.25\text{‰}^{\dagger, \Omega}$	$-0.35$ to $-0.28\text{‰}^{\dagger}$	(Weyer et al., 2008)	-0.32‰
<b>Inventories [moles]</b>				
	(fixed)			
Oceanic C inventory	$4.0 \cdot 10^{18}$	$4.0 \cdot 10^{18}$	(Berner, 1982)	1-30
Oceanic S inventory	$42 \cdot 10^{18}$	$42 \cdot 10^{18}$	(Berner, 1982)	0.05-1.0
Oceanic U inventory	$1.9 \cdot 10^{13}$	$1.9 \cdot 10^{13}$	(Dunk et al., 2002)	0.20-2.0
<b>Isotope compositions</b>				
$\delta^{13}\text{C}$ marine DIC pool	0.5‰	0.5‰	(Saltzman and Thomas, 2012)	0.2‰
$\delta^{34}\text{S}$ marine $\text{SO}_4^{2-}$ pool	21‰	21‰	(Gill et al., 2011)	27‰
$\delta^{238}\text{U}$ marine $\text{UO}_4^{2-}$ pool	-0.38‰	-0.38‰	(Weyer et al., 2008)	-0.45‰

fi – These references do not necessarily assume steady state. †Because  $\delta^{238}\text{U}$  of oceanic input is not well known, we assume  $\delta^{238}\text{U}$  is similar to crustal rocks (basalt and granites). These are constrained by only a handful of basaltic ( $\delta^{238}\text{U} = -0.37 \pm 0.07$ , 1SD, n = 4) and granitic ( $\delta^{238}\text{U} = -0.35 \pm 0.11$ , 1SD, n=4) samples (Weyer et al., 2008).  $\Omega$  – The isotope composition of the oceanic inputs are chosen to meet steady state at modern-day seawater composition.

**Table S3: Average isotope fractionation factors and isotope compositions of the oceanic input in the model**

	$\Delta^{13}\text{C} = \delta^{13}\text{C}_{\text{sw}} - \delta^{13}\text{C}_{\text{sink}}$	$\Delta^{34}\text{S} = \delta^{34}\text{S}_{\text{sw}} - \delta^{34}\text{S}_{\text{sink}}$	$\Delta^{238}\text{U} = \delta^{238}\text{U}_{\text{sw}} - \delta^{238}\text{U}_{\text{sink}}$
<b>Sink</b>			
Deltaic sediments	28‰	35‰	-0.19 <sup>†</sup>
High productivity, anoxic	26‰	35‰	-0.50
High productivity areas, oxic waters	28‰	35‰	-0.19
Low productivity areas	28‰	35‰	-
Carbonates, from anoxic pore fluids	Organic C: 28‰ Inorganic C: 0‰	Sulfate: 0‰	-0.27
Carbonates, from oxic waters	0‰	Sulfate: 0‰	-0
Evaporites (oxidized S)	-	0‰	-
Basaltic Alteration (U)	-	-	?
Ferromanganese Crusts (U)	-	-	+0.15 <sup>f</sup>

Abbreviations: sw = seawater. References: C isotopes (Gill et al., 2011), S isotopes (Gill et al., 2011), and U isotopes (see summary in main text). <sup>†</sup> The  $\delta^{238}\text{U}$  of deltaic sediments have not yet been measured and are assumed to have similar composition as sediments deposited under oxic high productivity settings. <sup>f</sup> (Brennecke et al., 2011; Weyer et al., 2008).

## S2.1 Model perturbation of fluxes

The burial event was modeled by modulating the sink fluxes in equation 1 and 2 from its initial state ( $J_0$ ) adding a positive perturbation ( $J'$ ),

$$\text{(eq. S4)} \quad J = J_0 + J'$$

Implicitly, we assume that enhanced burial fluxes were driven by independent external factors (e.g. enhanced organic preservation, primary production, expanding anoxia) – decoupled from changes in oceanic C, S and U inputs. This can be justified on the basis that Earth system models show that P availability (external factor in our model) exerts stronger control on global organic carbon burial than does the total oceanic carbon input (Van Cappellen and Ingall, 1994). More realistic models (with a terrestrial cycle) should explore modulations and potential negative feedbacks associated with the driving force.

Mathematically, two differentiable functions were used to simulate the burial perturbation. This was done mainly to avoid any unrealistic burial rates at the onset and termination of the event, and to explore the nature of the forcing function:

Gaussian perturbation:

$$\text{(eq. S5a)} \quad J' = A_i \exp[-(t-t_{\text{Pert}})^2/(2 \sigma_t^2)]$$

Logistic step perturbation:

$$\text{(eq. S5b)} \quad J' = A_i \cdot [1 + \exp(-(t - (t_{\text{Pert}} - \Delta t/2))/\sigma_t))]^{-1} \cdot [1 + \exp(-(t - (t_{\text{Pert}} + \Delta t/2))/\sigma_t))]^{-1}$$

Here,  $A_i$  is the magnitude of the sink expansion for the  $i^{\text{th}}$  setting (i.e. deltaic sink, oxic high productivity sink, and anoxic sinks). The magnitude can be thought of either as an areal expansion relative to the Cambrian state at constant mass accumulation rate or enhanced mass accumulation with an areal expansion smaller than  $A_i$ . The time mid-point of the event and the duration of the perturbed state is  $t_{\text{pert}}$  and  $\Delta t$ , respectively. The time to transit into the perturbed state ( $\sim\sigma_t$ ) also determines the duration of the Gaussian event ( $=2\sigma_t$ ). For the step-wise amplification,  $\sigma_t$  is shorter than the duration of the burial episode, so that the duration of the burial event is approximately given by  $\Delta t$ .

## S2.2 Fitting the scenarios for the burial event to observed data

To evaluate scenarios representative of the observed geochemical data, we evaluated our modeling solutions on eleven data constraints related to the magnitude, shape, and timing of the observed isotope excursions:

- (1) The  $\delta^{238}\text{U}$  excursion peaks before  $\delta^{13}\text{C}$  peaks
- (2) The  $\delta^{238}\text{U}$  excursion peaks before  $\delta^{34}\text{S}$  peaks
- (3) The  $\delta^{34}\text{S}$  excursion peaks before  $\delta^{13}\text{C}$  peaks
- (4) The  $\delta^{238}\text{U}$  excursion terminates roughly near the peak of the  $\delta^{13}\text{C}$  excursion
- (5) The  $\delta^{238}\text{U}$  excursion terminates roughly near the peak of the  $\delta^{34}\text{S}$  excursion
- (6) The magnitude of the  $\delta^{13}\text{C}$  excursion is 4-6‰
- (7) The magnitude of the  $\delta^{34}\text{S}$  excursion is 20-30‰
- (8) The magnitude of the  $\delta^{238}\text{U}$  excursion is  $-0.18\pm 0.02\%$
- (9) The characteristic decay time for the C and U isotope profiles were indistinguishable:  $t_C/t_U \approx 1$
- (10) The characteristic decay time for the S and U isotope profiles were indistinguishable:  $t_C/t_U \approx 1$
- (11) The magnitude of S isotope fractionation during pyrite formation in the Whelan basin,  $\Delta^{34}\text{S}_{\text{local}}$ , is -35‰ at the onset of the  $\delta^{238}\text{U}$  excursion.
- (12)  $\Delta^{34}\text{S}_{\text{local}}$  declines to 0 where  $\delta^{238}\text{U}$  excursion terminates.

We started our modeling exercises assuming simplest scenarios first.

### Case 1: One-stage burial event in anoxic high-primary productivity zones

First, we explored scenarios where the anoxic sink was enhanced during one single anoxic burial episode. This scenario did not permit a simultaneous fit of the amplitude of all the isotope excursions (criteria 5-7) (Figure 4). Typical magnitudes for the  $\delta^{13}\text{C}$  and  $\delta^{34}\text{S}$  excursions needed to produce a  $\delta^{238}\text{U}$  excursion with magnitude of  $-0.18\%$  were only  $+0.1\%$ , much less than that observed from the C and S isotopic records. Conversely, a single burial episode in deltaic settings would approximately fit the magnitudes for the  $\delta^{13}\text{C}$  and  $\delta^{34}\text{S}$  (if we assume a rather low C/S = 1.0 versus the modern C/S of 2.8; Alum shale C/S = 1.5-1.8), but this was not sufficient to produce the magnitude of the U excursion ( $-0.02\%$ ).

### Case 1 variant: One-stage burial event in oxic high-productivity settings (equiv. to modern OMZ's)

Model simulations with enhanced burial in oxic high primary productivity settings (oxHPP) are shown in Figure S2. These scenarios simultaneously promote carbon,

sulfur and uranium burial on the continental shelves (Table 1). Likely, Cambrian deltaic settings were very different from today prior to the invasion of vascular plants on the continents, for example with lower overall mass accumulation rates. Perhaps, burial rates in sediments in the mixed layer of the ocean would closer resemble modern oxic primary productivity settings than modern deltaic settings. However, the scenarios in Fig. S2 illustrate that extensive organic C and pyrite S burial with concomitant U burial in these settings cause massive U draw down, contradicting observations from the Alum shale basin where constantly high U accumulation and enhanced marine U levels (decoupled from the isotope excursion) can be inferred (Figure 7).

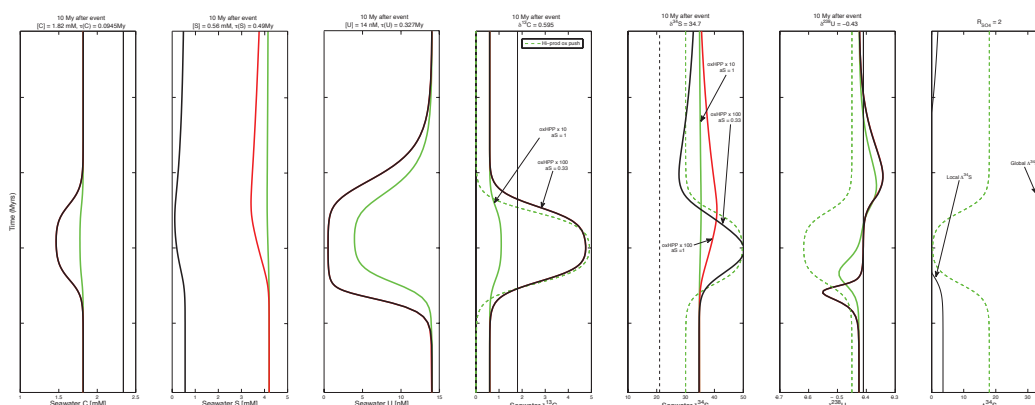


**Figure S2. Three examples of one-stage burial scenarios with expanded burial beneath oxic high primary productivity zones (oxHPP). A 10-fold expansion (green solid curves) yields only a small U isotope excursion, whereas a 100-fold expansion (black) would fit the magnitude. A slow response between S burial flux and inventory ( $a_S = 0.33$ ) would fit the relative timing of the isotope peaks, incl.  $\delta^{34}\text{S}$ . However, the early U isotope peak is grounded in dramatic drawdown of oceanic U, inconsistent with the constantly high U enrichments in the Alum basin (Fig. 7). In all cases, the  $C/S = 1.0$  is set to a minimum in order to maximize the magnitude of the  $\delta^{34}\text{S}$  excursion.**

## Case 2: One-stage burial event in both anoxic high-primary productivity zones and deltas

The acceptable modeling solutions were produced when burial fluxes into both anoxic settings and shallow oxygenated deltaic sediments simultaneously increased (introducing additional model parameters  $A_{i,\text{anoxic}}$  and  $A_{i,\text{deltas}}$ ).

More than 100 simulations were run and several solutions were able to fit the magnitude and relative timing of the peaks. Only portions of solution space are illustrated here (Table S4-S5). The boundary conditions for the initial Cambrian ocean state were allowed to vary. Most solutions have large DIC and small  $\text{SO}_4^{2-}$  reservoirs, whereas the U concentration in seawater could vary over a broad range of values.

Both the amplitude criteria (5-7) and isotope peak displacement criteria (1-4) were met when anoxic and deltaic sink fluxes increased 5–8 and 1–3 times their pre-event values (Table S4), respectively.

Displacements between C-U and S-U isotope peaks (criteria 9-10) occur even in one-stage burial scenarios, when the oceanic C and S inventories are relatively large compared to that of U (Figure 5). However, these model solutions have different shape (i.e. decay time) compared to the observed isotope excursions and the timing of the waning S isotope fractionation signal is off (criteria 11). All the isotope data are from the same drill core, so there is no stratigraphic mismatch and the relative timings of the isotope curves are well preserved. Models show a slower decay time of the isotope excursions for elements with a longer residence time. This contradicts the estimated characteristic decay time in the Mt. Whelan profiles that are indistinguishable from one another (see signal analysis in section S3).

### Case 2 variants

There are several parameters that affect the decay time scale and relative timing of the peaks; for example the response between fluxes and inventories ( $a_i$ ) and inventory-dependent fractionation factors.

#### *Rapid burial at low marine inventories*

Figure S3 shows a scenario where a slow response of the S burial flux to decreasing sulfate concentrations ( $a_S = 0.5$ , dashed) generates a faster isotope decay profile than a fast response ( $a_S = 1$ , solid). Thus, a slower burial response in the S cycle than in the U cycle would better fit the decay time scale. However, this has a side effect – it decreases the displacement between the isotope peaks.

#### *Fractionation factors vary with sulfate inventory*

Figure S4 shows a model solution where global S and U isotope fractionations ( $D_i$ ) depend on oceanic sulfate inventory  $[\text{SO}_4^{2-}]_{\text{ocean}}$ , when marine sulfate levels decrease below a threshold value  $[\text{SO}_4^{2-}]_{\text{muted}}$ .

$$\begin{aligned} \text{(eq. S6)} \quad \Delta_i &= \max \{ \Delta_{\text{max}} ; a_i \cdot [\text{SO}_4^{2-}]_{\text{ocean}} + b_i \} \\ \text{where} \quad a_i &= (\Delta_{\text{max}} - \Delta_{\text{min}}) / ([\text{SO}_4^{2-}]_{\text{muted}} - [\text{SO}_4^{2-}]_{\text{none}}) \\ b_i &= \Delta_{\text{min}} - a_i \cdot [\text{SO}_4^{2-}]_{\text{none}} \end{aligned}$$

Here,  $[\text{SO}_4^{2-}]_{\text{muted}} = 2 \text{ mM}$  and  $[\text{SO}_4^{2-}]_{\text{none}} = 0.1 \text{ mM}$  are the sulfate concentration thresholds at which muted isotope fractionations begin and become fully expressed, respectively. Alternatively, muted isotope fractionations were declining as a logarithmic function of sulfate levels (consistent with Habicht et al. 2002 for S isotope fractionation):

$$\begin{aligned} \text{(eq. S7)} \quad \Delta_i &= \max \{ \Delta_{\text{max}} ; a_i \cdot \log([\text{SO}_4^{2-}]_{\text{ocean}}) + b_i \} \\ \text{where} \quad a_i &= (\Delta_{\text{max}} - \Delta_{\text{min}}) / \log([\text{SO}_4^{2-}]_{\text{muted}} / [\text{SO}_4^{2-}]_{\text{none}}) \\ b_i &= \Delta_{\text{min}} - a_i \cdot \log([\text{SO}_4^{2-}]_{\text{none}}) \end{aligned}$$

The maximum isotope fractionations ( $\Delta_{\text{max}}$ ) were chosen for each isotope system (S or U) and each environmental setting at their maximum value (Table S2). The minimum isotope fractionations ( $\Delta_{\text{min}}$ ) were set to zero.

The local S isotope fractionation signature in the Mt Whelan sediments were calculated using equations 6 and 7, but with the sulfate concentration in the pyrite forming zone of the Whelan sediments instead of the open ocean value. To simulate

the shape and timing of the  $\Delta^{34}\text{S}$  curve during the event, the sulfate concentration in the sediments is assumed at fixed proportion ( $R_{\text{SO}_4}$ ) of open ocean concentration:

$$\text{eq. S8} \quad [\text{SO}_4^{2-}]_{\text{sediments}} = [\text{SO}_4^{2-}]_{\text{ocean}}/R_{\text{SO}_4}$$

Preferentially, a two-stage scenario with faster S burial response to inventory change can fit the relative timing of the peaks and the similar decay time scales. The isotope peaks occur earlier without significantly changing the characteristic decay time scale. Therefore, if U isotope fractionation was sulfate dependent, then the U isotope peak may precede the S and C isotope peaks. In section S1, we argued that U isotope fractionation might be sulfide dependent. Hence, this solution is consistent with our expectation for an event that transitioned from euxinic to ferruginous anoxic settings as a result of sulfate draw down the SPICE event. We consider this an example of a two stage burial episode, and we explore more 2-stage scenarios below.

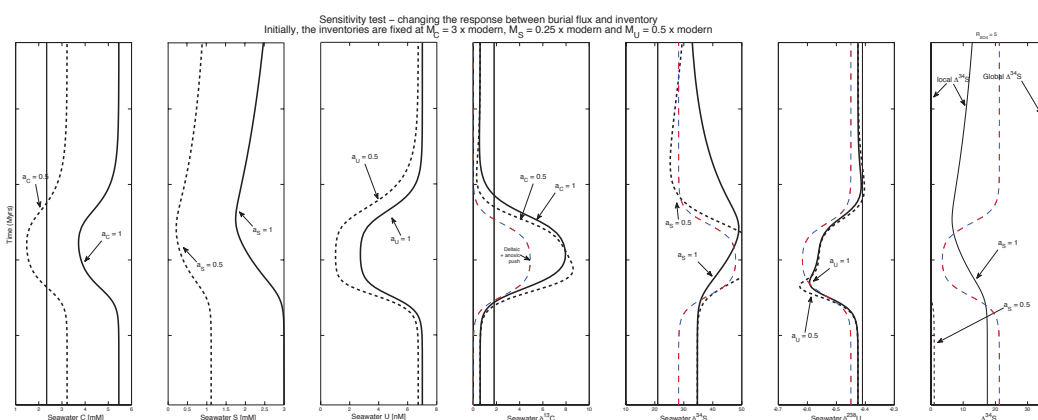


**Figure S3. A one-stage burial scenario with strong (black, dashed,  $a_C = a_S = a_U = 1$ ) and weak (black, solid,  $a_C = a_S = a_U = 0.5$ ) inventory dependency on burial fluxes in all settings ( $J = b \cdot M^a$ ). All model details in Table S5.**

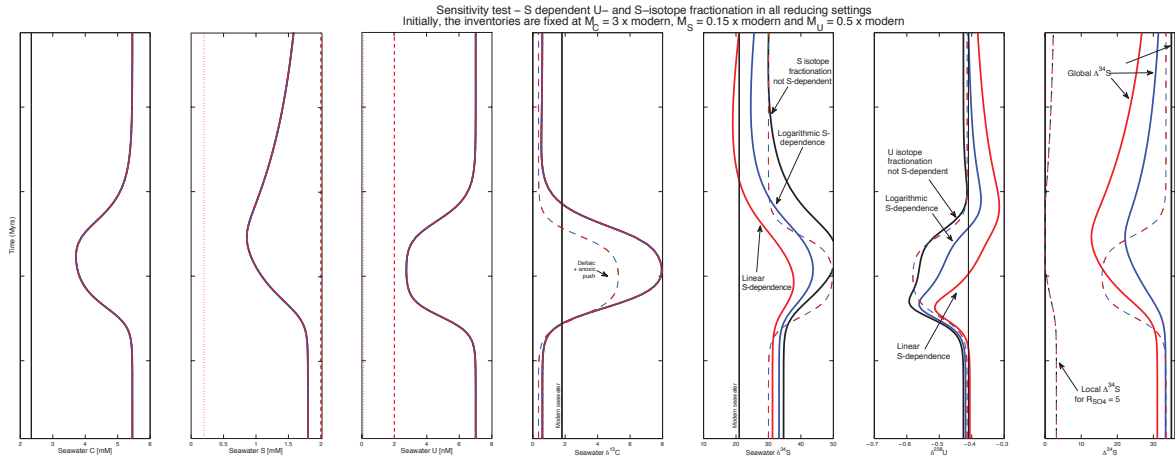


**Figure S4. One-stage burial scenarios with sulfate dependent S- and U isotope fractionation (global effects). The net U and S isotope fractionation factors in euxinic and other reducing settings are constant values above 2 mM oceanic  $\text{SO}_4^{2-}$  (0.50‰, 0.27‰ and 1.9‰ for U in euxinic, sulfidic carbonates and SAD settings and constantly 35‰ for S in all reducing settings). Isotope fractionation decline linearly (red)/logarithmically (blue) from 2 to 0.1 mM and there is no fractionation expressed below 0.1 mM oceanic  $\text{SO}_4^{2-}$  (eq. S6 and S7). All model details are given in Table S5.**

### Case 3: Two-stage burial event in anoxic and oxic high-primary productivity zones followed by burial only in (oxygenated) deltas

A burial episode that includes continued burial in oxygenated high-productivity settings (e.g. equivalent to modern deltas) can also fit the acceptable model solution criterion. As in case 2, the isotope excursions can be recreated when burial fluxes into both anoxic settings and shallow oxygenated deltaic sediments simultaneously increase. However acceptable solutions can be generated by continuing burial in deltas for a longer period of time. This introduces one additional parameter that distinguishes the duration of the anoxic event ( $\Delta t_{\text{OAE}}$ ) and the deltaic expansion ( $\Delta t_{\text{deltas}}$ ).

Figure S5 shows a modeling solution that fits all constraints including the peak shift and quick  $\delta^{13}\text{C}$  decline. Here the deltaic expansion continues twice as long as the duration of the anoxic expansion. The C-U isotope peak shift is the result of a massive DIC pool (37 mM, 16-fold increase relative to modern ocean). The rapid isotope decay occurs because of C and S fluxes are not linearly coupled to declining C and S inventories, whereas U fluxes are coupled to the marine U inventory; i.e.  $1 = a_U > a_C = a_S$ . Model parameters are listed in Table S4. Many other perturbations (shorter/longer duration, faster/slower onset, larger amplitudes, changing C/S during event, etc.) listed in Table S5 may also fit shape of the curves with extended deltaic burial episode, under the assumption that  $a_S < a_U$  and the DIC pool ( $M_C$ ) was greater than today.

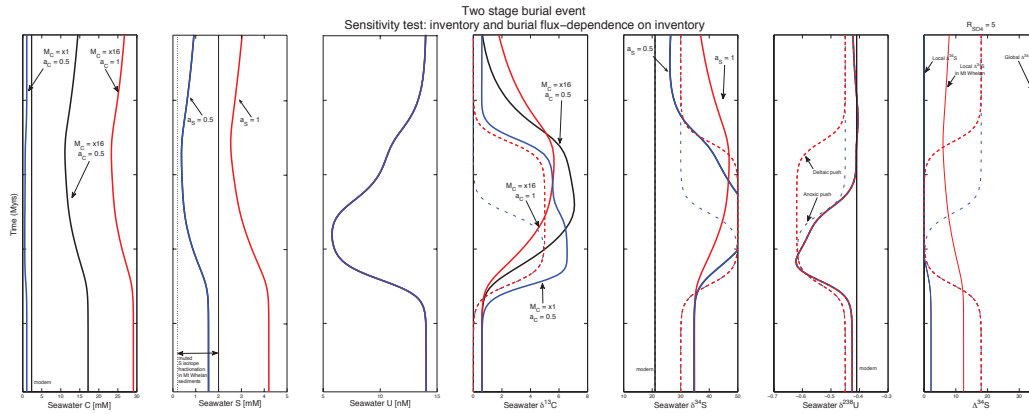


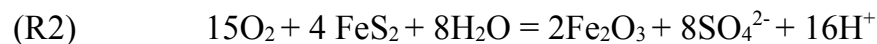
**Figure S5. Two-stage model solution with an extended deltaic (C-S and no U) burial episode after the anoxic event. Magnitudes, peak timings and decay profiles match (at least qualitatively) the observations from the Mt. Whelan drill core. In the modeled solution (black), the DIC pool is initially 16 times modern concentrations (=37 mM). Also, the C and S burial responses to the C and S inventories are weaker than for U ( $a_C = a_S < a_U$ ). The effect of a smaller DIC pool (blue) and faster C and S flux-inventory response ( $a_C = a_S = a_U = 1$ ) are shown (red). The scenario shown in black is identical to Fig. 6, except that muted S isotope fractionations only occur below 1 mM sulfate. All model details in Table S5.**

## S2.2. O<sub>2</sub> release after organic carbon and pyrite burial in CSU model

The delivery of oxidants to the surface environment from the marine C and S cycles is calculated in the CSU model assuming enhanced burial of organic C and pyrite S results in the accumulation of O<sub>2</sub> in the Earth's atmosphere and oceans, according to the following two reactions:



Reading equation R1 from right to left, this reaction represents the burial in sediments of organic matter formed ultimately by photosynthesis. Going from left to right, the reaction represents either oxidative weathering of old of organic matter in the crust or thermal decomposition of organic matter ultimately released as gas to the atmosphere and oceans. Importantly, 1 mol C buried in the crust releases 1 mol of O<sub>2</sub> (Berner, 2001).



Reading equation R2 from left to right, this reaction represents oxidative weathering of pyrite in the crust or thermal decomposition of pyrite at depth with the resulting sulfur gasses released to the atmosphere and oceans. Going from right to left represents pyrite burial in sediments formed ultimately by sulfate reducing bacteria. Importantly, 8 moles S buried in the crust release 8 moles of O<sub>2</sub> to the atmosphere and oceans (Berner, 2006).

In our perturbation model, all C and S removal from the ocean comes from the burial of reduced C and S. Thus, the O<sub>2</sub> production is simply computed from the marine C

and S draw down, as the integral over the C and S removal over the course of the event(s):

$$(eq. S9a) \quad \Delta(O_2)_{\text{fromC}} = -1/1 \int (dM_C/dt) dt$$

$$(eq. S9b) \quad \Delta(O_2)_{\text{fromS}} = -15/8 \int (dM_S/dt) dt$$

**Table S4: Favored parameter values that simultaneously fit the  $\delta^{13}\text{C}$ ,  $\delta^{34}\text{S}$  and  $\delta^{238}\text{U}$  isotope excursion amplitude constraints.<sup>†</sup> Not all combinations of the parameters produce acceptable solutions. See Table S5 for specific model details.**

Parameter	Fig. 6	Range	Units
Anoxic sink amplification, $A_{\text{anoxic}}$	5	5-8	Pre-event value
Deltaic sink amplification, $A_{\text{deltaic}}$	1.2	1-3	Pre-event value
Duration, $\Delta t_{\text{anoxic}}$	0.96	0.96	Myr
	0.96	0.96-1.92	
Sigma, $\sigma_t$	0.1	0.1	Myr
C/S mass ratio, CS	1.0	1-2.8	g/g
Initial marine C inventory, $M_C^{\epsilon}$	16	16-30	Modern-day
Initial marine S inventory, $M_S^{\epsilon, \S}$	0.5	0.1-0.5	Modern-day
Initial marine U inventory, $M_U^{\epsilon}$	1.0	0.5-1.0	Modern-day
Marine C input, $J_C$	1.0	0.4-1.0	Modern-day
Marine S input, $J_S$	1.0	0.4-1.0	Modern-day
Marine U input, $J_U$	1.0	0.4-1.0	Modern-day
Inventory sensitivity of C burial fluxes, $a_C$	1.0	0.5-1	
Inventory sensitivity of S burial fluxes, $a_S$	0.3	0.3-1	
Inventory sensitivity of U burial fluxes, $a_U$	1.0	0.5-1	

<sup>†</sup>Modern C/S mass ratio in all reducing sinks is 2.8. <sup>‡</sup>An exhaustive search of solution space have not been performed. <sup>ϵ</sup>The oceanic inventories vary and settle to a steady state before and after the event. These are the initial values used to initiate the Cambrian simulations. The derived Cambrian inventories are shown in figures 4-6, S2-S5 and depend on the source and sink fluxes and specifically how the sink fluxes respond when inventories decline ( $a_i$ ). <sup>§</sup>Note that the marine S inventories also decrease from this initial value, when the C/S in reducing sediments is less than the modern value (=2.8 by mass).

**Table S5. A summary of parameter values and model output for various scenarios illustrated in Figs. 4-6, S2-S5 and other models summarized in Table S4.**

(TableS5\_Model\_scenarios.xlsx)

**Table S6. A summary of published U isotope data and the reference materials in use. Although a range of certified reference materials are used, the most common reference materials (SRM-950a, CRM-145, and CRM-112a formerly known as SRM-960) all have indistinguishable  $^{238}\text{U}/^{235}\text{U}$  ratios (Condon et al., 2010; Jacobsen et al., 2009). This allows for direct inter-laboratory comparison of  $\delta^{238}\text{U}$  values generated in different studies and laboratories, despite a lack of consensus on absolute  $^{238}\text{U}/^{235}\text{U}$  values.**

(TableS6\_Published\_d238U\_terrestrial\_rocks.xlsx)

### S3. The reservoir effect – isotope peak displacement during one burial event

The 'reservoir effect' can produce displacement between the C-S and U isotope excursions because the element with longest marine residence times would peak last, as exemplified with the carbon-sulfur-uranium models (e.g. Fig. 5). Yet, a close examination of the Mount Whelan isotope profiles causes us to conclude that the displacement is not generated in the reservoir effect. Here, we summarize how this interpretation comes about.

Suppose three elements are buried together in ocean sediments at elevated rates, and that the burial episode stops all three fluxes simultaneously. The reservoir effect will then cause the isotope composition of the element with longest residence time to decay slower. The slow washout shows up in the falling limbs of the  $\delta^{13}\text{C}$  and  $\delta^{34}\text{S}$  excursions. We can define the characteristic time scale of the isotope decline as follows:

$$\text{(eq. S10)} \quad t = - \delta' / (d \delta / dt)$$

where  $\delta'$  is the isotopic offset relative to steady state value. The characteristic time scale is mathematically equivalent to the residence time of the element, when equation S10 is evaluated at the termination datum of the burial episode (e.g.  $J_{\text{org}} = 0$ ) (see subsection S3.1 for derivation).

In this section S3.6, we perform signal analysis to show that the ratios between characteristic decay time scales in the Mt. Whelan isotope profiles are indistinguishable from one another ( $\tau_{\text{C}}/\tau_{\text{S}} = 2.3 \pm 1.3$ ,  $\tau_{\text{C}}/\tau_{\text{U}} = 2.1 \pm 1.2$ , and  $\tau_{\text{S}}/\tau_{\text{U}} = 0.9 \pm 0.5$ ). This is not what we would expect to observe if the 'reservoir effect' was the only cause for the offset between the isotope profiles. In contrast, the similar characteristic time scales are expected if the perturbed burial rates relaxed over longer time scales than the residence time of all involved elements;  $\tau_{\text{C}}, \tau_{\text{S}}, \tau_{\text{U}} > 100$  kyrs. Thus, this is conceptually consistent with a two stage burial episode where U and C-S burial were decoupled in time (Fig. 6).

#### S3.1 Burial events and isotope excursions

In a simple 1-box ocean model the elemental and isotope mass balances for any element with reducing and oxidizing sinks (e.g. C, S and U) read:

Mass balance

$$\text{(eq. 11)} \quad dM/dt = J_{\text{w}} - J_{\text{ox}} - J_{\text{red}}$$

Isotope mass balance

$$\text{(eq. S12)} \quad d(M \delta) / dt = \delta_{\text{w}} J_{\text{w}} - \delta_{\text{sw}} J_{\text{ox}} - J_{\text{red}} (\delta_{\text{sw}} - \Delta_{\text{red-sw}})$$

Here,  $M$  is the oceanic inventory of the focal element,  $d_i$  and  $J_i$  are the isotope composition and flux of the major sources and sinks ( $i$ ) – weathering input ( $W$ ), total burial flux in reducing settings (e.g. organic carbon burial) and oxidizing settings (e.g. carbonate burial with  $\delta_{\text{carb}}$  and  $\delta_{\text{sw}}$  of seawater), respectively. Note, in contrast to eq.

1 and 2, we have now simplified the equation to include all reducing sinks and oxidizing sinks as two sinks with distinct isotope compositions, respectively.

Using the product rule " $d(M\delta)/dt = M d(\delta)/dt + \delta \cdot d(M)/dt$ ", equations S11 and S12 combine to:

$$(eq. S13) \quad J_{red} = 1/\Delta_{red-sw} [ J_w (\delta_{sw} - \delta_w) + d \delta_{sw}/dt M ]$$

The first term in eq. S13 is always positive and the sign of the second term is determined by the gradient of the isotope curve. The left hand side is always positive, since burial fluxes are positive, requiring that the modulus of the second term inside the paranthesis is a fraction of the first term when  $d \delta_{ox}/dt < 0$ , e.g. on the falling limb of an isotope excursion.

### S3.2 Perturbation theory – consequence of a burial event

A significant displacement between the peak of  $J_{red}(t)$  and  $d_{sw}(t)$  can be represented by the second term in equation S13 being large and negative. This represents the reservoir effect as it is expressed in the isotope profile. Here, we show mathematically how the element with longest residence time necessarily also has the largest reservoir effect.

First, we describe the change in  $\delta$  and  $J_{red}$  as perturbations from steady state. This is written in terms of constant and a time dependent term (with prime). Formally, it means:

$$(definition) \quad \delta = \delta_0 + \delta' \text{ corresponds to a change in } J_{red} = J_{red,0} + J_{red}'$$

Inserting the definitions  $\delta_{sw} = \delta_0 + \delta'$  and  $J_{red} = J_{red,0} + J_{red}'$  into eq. S13 and invoking the sum rule for  $d(\delta_0 + \delta')/dt = d\delta_0/dt + d\delta'/dt$ , and noting that  $d\delta_0/dt = 0$  and  $J_{red,0}/J_w = (\delta_0 - \delta_w)/\Delta_{red-sw}$  outside the perturbation, we find:

$$(eq. S14, eq. 4) \quad \delta' = \Delta_{red-sw} J_{red}'/J_w - M/J_w d\delta'/dt$$

Here, we have also used that  $J_{red-sw,0}/J_w = (\delta_0 - \delta_w)/\Delta_{red-sw}$  outside the perturbation. Thus,  $\delta_0$  represents the isotope composition of seawater outside the event, when fluxes are at steady state.

### S3.3. Displacement between isotope profiles by the reservoir effect

The second term in eq. S14 determines the ‘reservoir effect’ that, for example, describes the delayed response of the oceanic  $\delta^{13}C$  curve relative to the period of enhanced organic C burial; i.e. the shift between isotope peaks or zero crossings of  $\delta^{13}C$  relative to  $J_{org}$ .

Equation S14 also shows that the organic carbon burial flux ( $J_{org}$ ) and carbonate  $\delta^{13}C$  will co-vary (no reservoir effect), when the second term is negligible relative to the first term and provided weathering input ( $J_w$ ) and isotope fractionation ( $\Delta_{red-sw}$ ) do not significantly change.

Similar relationships hold for the S and U cycle. For example, we can write

$$\text{(eq. S14U)} \quad -\delta_U' = \Delta_{\text{anox-sw}} J_{\text{anox,U}}' / J_{\text{w,U}} - M_U / J_{\text{w,U}} d(-\delta_U')/dt$$

Here,  $D_U$  is the magnitude of isotope fractionation during anoxic burial relative to seawater composition (+0.4-0.6‰),  $M_U$  is the marine U inventory,  $J_{\text{anox,U}}'$  is the perturbation of the global anoxic U burial flux and  $J_{\text{w,U}}$  is the U input flux via weathering. Note that  $-\delta_U$  and  $d(-\delta_U')/dt$  are initially increasing functions of time.

Because  $M/J$  in the second term is relatively large in the equation for C (eq. S14) relative to the equation for U (eq. S14U), a significant isotope peak displacement between the C, S and U isotope profiles is to be expected even when enhanced burial fluxes C, S and U are correlated and terminate simultaneously as in the “one-stage” burial scenario.

### S3.4 Marine oceanic residence time

The marine residence time of an element is defined by the ratio of the oceanic inventory to the total input/output flux. It determines the characteristic time scale on which the inventory can be refilled after exhaustion and represents the time to reach steady state after a perturbation is induced to the steady state where fluxes balance.

$$\text{(definition)} \quad t = M/J_w$$

In principle, the instantaneous residence time (at any given time point) can be derived directly from the isotope curve, if we know when the enhanced burial episode terminated. This is clear from evaluating eq. S14 at the time when enhanced burial in reducing settings terminated,  $J_{\text{red}}'(t = t_{\text{term}}) = 0$ . This gives:

$$\text{(eq. S15)} \quad M(t_{\text{term}})/J_w(t_{\text{term}}) = -\delta'(t_{\text{term}})/(d\delta'/dt)|_{t_{\text{term}}}$$

The left hand side is the mathematical definition of residence time at  $t = t_{\text{term}}$ :

$$\text{(eq. S16)} \quad t(t_{\text{term}}) = -\delta'(t_{\text{term}})/(d\delta'/dt)|_{t_{\text{term}}}$$

Here, subscripts (C, S, U) are omitted, because the equations generally apply to all three isotope systems. It is important to note that the termination of the burial episode necessarily occurs within the falling limb of the isotope excursion (because  $\delta' > 0$  requires  $(d\delta'/dt) < 0$ , since  $t$  and  $\delta'$  are always positive at that point). Due to the reservoir effect the termination occurs at a time point where there is still a non-zero isotope excursion.

With this in mind, we can now compare multiple isotope profiles to see if the record allows simultaneous termination of the burial episode of the various elements. Indeed, the  $\delta^{13}\text{C}$  profile show that the excursion terminates above  $z = 82.5$  m depth in the Mt Whelan drill core The U isotope excursion ends at  $\sim 99$  m depth and cannot be determined above  $\sim 75$  m where local U isotope fractionation change erratically. This leaves a relative narrow window from 75 to 82.5 m for a possible common termination datum in the Whelan section (Fig. S6).



### S3.6 Estimating the stratigraphic residence times from the isotope profiles

We determined  $h$  directly from the isotope curves in the Mt. Whelan drill core, given the uncertainties associated with termination datum and steady-state  $d$ . The first derivative was calculated using a smoothing function with one free parameter,  $r$ , which determines the relative weight placed on the contradictory demands of having the spline curve smooth ( $\rho = 0$ ) vs. having it close to data ( $\rho = 1$ ). We picked relatively low values for  $\rho$  to avoid small oscillations overlain on the overall excursions (Fig. S7).

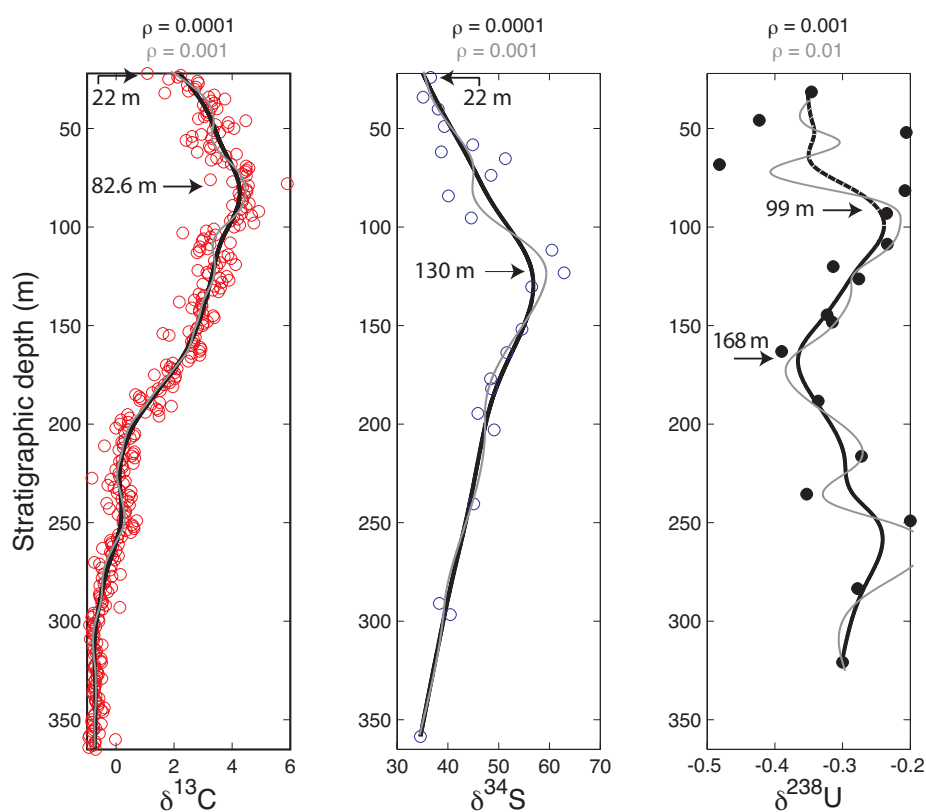


**Figure S7. Smoothed spline fits through data used to derive the first derivative, and stratigraphic residence time. Smoothed spline fits using lower  $r$ -values (grey) picks up small oscillations in the overall isotope excursion. Thus, these are ignored in the residence time calculation.**

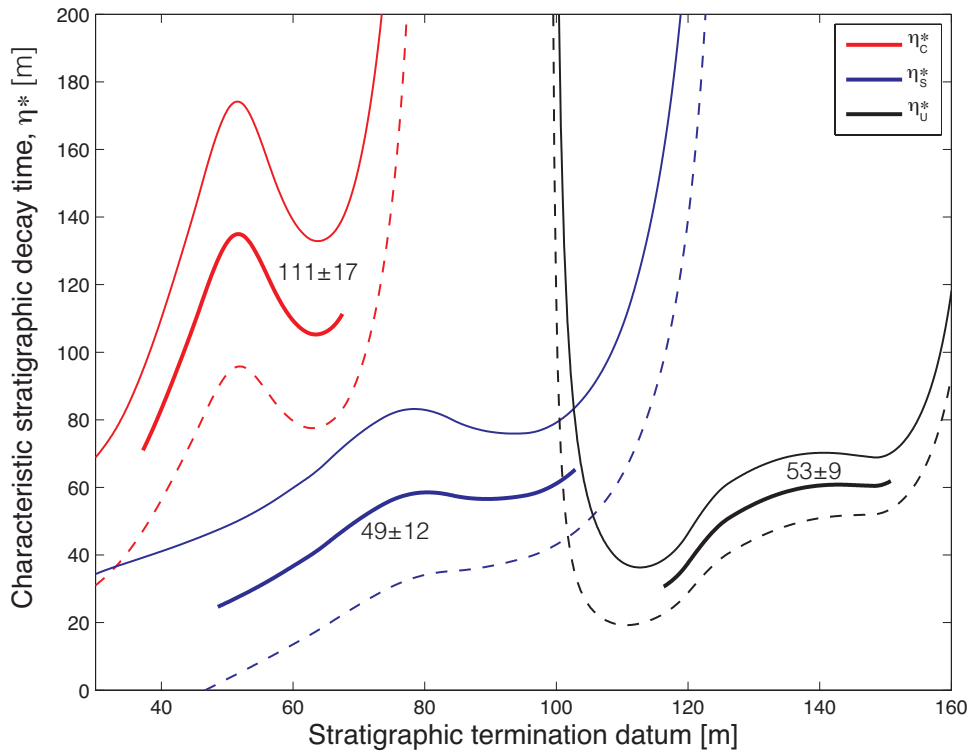


**Figure S8.** The stratigraphic residence time of C, S, and U (eq. S17) obtained from the smoothed isotope profile (Fig. S7) of the Mt. Whelan data. The favored values is highlighted with a thick curve using steady state isotope compositions in marine carbonates  $\delta^{13}\text{C} = 0 \pm 1\text{‰}$ ,  $\delta^{34}\text{S} = 35 \pm 5\text{‰}$ , and  $\delta^{238}\text{U} = -0.18 \pm 0.02\text{‰}$  (anoxic carbonates). The thin lines represent the error envelope associated with uncertainties of the steady-state isotope composition of seawater (e.g. prior to the event), and the x-axis shows how  $h$  varies as a function of choice of termination datum. We see this corresponds to  $\sim 50\%$  uncertainty on the  $h$  estimates. Above 100 m depth, the U isotope curve is not representative of secular variations in seawater chemistry, which means the stratigraphic residence time (= characteristic residence time evaluated at the termination of the burial episode) cannot be evaluated at a common stratigraphic level. This may well be because the enhanced burial fluxes of C, S and U did not terminate simultaneously (discussed further in section S3.7).

Our analysis shows that the characteristic decay time scales of isotope profile for U is similar to those obtained for C and S. We assume termination falls somewhere at the midpoint of the falling limb  $\pm 1/4$  width (thick lines in Fig. S8), yielding stratigraphic residence times with mean and standard deviation of  $\eta_C = 111 \pm 17$  m,  $\eta_S = 49 \pm 12$  m, and  $\eta_U = 53 \pm 9$  m. Here, the uncertainties from the steady state isotope compositions in the ocean are estimated at  $\delta^{13}\text{C} = 0 \pm 1\text{‰}$ ,  $\delta^{34}\text{S} = 35 \pm 5\text{‰}$ , and  $\delta^{238}\text{U} = -0.18 \pm 0.02$  (anoxic carbonates). This leads to indistinguishable characteristic decay time scales:  $\tau_C/\tau_S = 2.3 \pm 1.3$ ,  $\tau_C/\tau_U = 2.1 \pm 1.2$ , and  $\tau_S/\tau_U = 0.9 \pm 0.5$ .

This result is unexpected if the isotope peak displacement occurred as a result of the reservoir effect in a one-stage burial event (co-variation of perturbed C, S and U burial fluxes). Our forward models suggest that a 4-25 times larger residence time for C and S than for U is sufficient to produce a significant isotope peak displacement. Yet, this should produce similarly longer characteristic decay time scales for C and S vs. U.

Instead, the offset between S and U isotope excursions appear to have distinct burial termination horizons. Strictly, this implies that enhanced pyrite burial continued after the anoxic U burial episode. Therefore, our conclusion is that the displacement of isotope peaks results from diachronous burial rather than large C and S 'reservoir' effects.

### **S3.7: Sedimentation rate bias underestimates stratigraphic C and S decay time scales relative to U.**

The ratios between residence time scales can be obtained for a one-stage scenario, so that the termination datum is simultaneous for all involved cycles. In our fitting exercise of the Mt. Whelan data (Fig. S7), the U isotope decay occurs before that of C and S. The sediment rates were higher during the U isotope excursion, which led to thicker stratigraphic packages (during the rising limbs of the  $\delta^{13}\text{C}$  and  $\delta^{34}\text{S}$  excursions, and not during the falling limbs of the  $\delta^{13}\text{C}$  and  $\delta^{34}\text{S}$  excursions). This is because, the time interval before the sea level low is a High Stand Systems Tract (HST) (Figure 7). The sequence boundary and maximum sea level low occurs at the peak of the  $\delta^{13}\text{C}$  excursion.

Sea level rise occurs above this horizon and during the falling limb of the  $\delta^{13}\text{C}$  excursion. This Transgressive Systems Tract (TST) is associated with slower sedimentation rates relative to the HST, causing a thinning of the stratigraphic packages. Therefore, the falling limbs of the  $\delta^{13}\text{C}$  and  $\delta^{34}\text{S}$  excursions are condensed in the stratigraphy relative to  $\delta^{238}\text{U}$  excursion. Thus, the obtained characteristic decay time scales could not be evaluated at the same termination datum. Thus, the estimated values for  $\eta_{\text{C}}$  and  $\eta_{\text{S}}$  could well represent more time relative to  $\eta_{\text{U}}$ , and the C and S residence time scales could be similar or greater than for U;  $\tau_{\text{C}}/\tau_{\text{U}} \geq 2.1 \pm 1.2$ , and  $\tau_{\text{S}}/\tau_{\text{U}} \geq 0.9 \pm 0.5$ .

## Supplementary references

- Bargar, J.R., Williams, K.H., Campbell, K.M., Long, P.E., Stubbs, J.E., Suvorovad, E.I., Lezama-Pacheco, J.S., Alessi, D.S., Stylo, M., Webb, S.M., Davis, J.A., Giammar, D.E., Blue, L.Y., Bernier-Latmani, R., 2013. Uranium redox transition pathways in acetate-amended sediments. *Proceedings of the National Academy of Sciences* 110, 4506–4511.
- Berner, R.A., 1982. Burial of Organic Carbon and Pyrite Sulfur in the Modern Ocean: its Geochemical and Environmental Significance. *Am J Sci* 282, 451–473.
- Berner, R.A., 2001. GEOCARB III: A revised model of atmospheric CO<sub>2</sub> over Phanerozoic time. *Am J Sci* 301, 182–204.
- Berner, R.A., 2006. GEOCARBSULF: A combined model for Phanerozoic atmospheric O<sub>2</sub> and CO<sub>2</sub>. *Geochimica et Cosmochimica Acta* 70, 5653–5664.
- Brenneka, G.A., Wasylenki, L.E., Bargar, J.R., Weyer, S., Anbar, A.D., 2011. Uranium isotope fractionation during adsorption to Mn-oxyhydroxides. *Environ Sci Technol* 45, 1370–1375.
- Dunk, R.M., Mills, R.A., Jenkins, W.J., 2002. A reevaluation of the oceanic uranium budget for the Holocene. *Chemical Geology* 190, 45–67.
- Gill, B.C., Lyons, T.W., Young, S.A., Kump, L.R., Knoll, A.H., Saltzman, M.R., 2011. Geochemical evidence for widespread euxinia in the later Cambrian ocean. *Nature* 469, 80–83.
- Goldberg, T., Archer, C., Vance, D., Thamdrup, B., McAnena, A., Poulton, S.W., 2012. Controls on Mo isotope fractionations in a Mn-rich anoxic marine sediment, Gullmar Fjord, Sweden. *Chemical Geology* 296–297, 73–82.
- Hua, B., Huifang, X., Terry, J., Deng, B., 2006. Kinetics of Uranium(VI) Reduction by Hydrogen Sulfide in Anoxic Aqueous Systems. *Environ. Sci. Technol.* 40.
- Langmuir, D., 1978. Uranium Solution-Mineral Equilibria at Low-Temperatures With Applications to Sedimentary Ore-Deposits. *Geochimica et Cosmochimica Acta* 42, 547–569.
- Lighty, R.G., Macintyre, I.G., Stuckenrath, R., 1982. *Acropora Palmata* Reef Framework: A Reliable Indicator of Sea Level in the Western Atlantic for the Past 10,000 Years. *Coral Reefs* 1, 125–130.
- Lovley, D.R., Roden, E.E., Phillips, E.J.P., Woodward, J.C., 1993. Enzymatic iron and uranium reduction by sulfate-reducing bacteria. *Marine Geology* 1113, 41–53.
- Romaniello, S., 2012. Incorporation and Preservation of Molybdenum and Uranium Isotope Variations in Modern Marine Sediments, School of Earth and Space Exploration. Arizona State University, Tempe, p. 143.
- Saltzman, M.R., Thomas, E., 2012. Carbon Isotope Stratigraphy, in: Gradstein, F.M., Ogg, J.G., Schmitz, M., Ogg, G. (Eds.), *The Geological Time Scale*. Elsevier, pp. 207–232.
- Saltzman, M.R., Young, S.A., Kump, L.R., Gill, B.C., Lyons, T.W., Runnegar, B., 2011. Pulse of atmospheric oxygen during the late Cambrian. *Proceedings of the National Academy of Sciences* 108, 3876–3881.
- Tucker, M.D., Barton, L.L., Thomson, B.M., 1998. Removal of U and Mo from water by immobilized *Desulfovibrio desulfuricans* in column reactors. *Biotechnology and Bioengineering* 60, 88–96.
- Van Cappellen, P., Ingall, E.D., 1994. Benthic phosphorus regeneration, net primary production, and ocean anoxia: A model of the coupled marine biogeochemical cycles of carbon and phosphorus. *Paleoceanography* 9, 677–692.

Weyer, S., Anbar, A.D., Gerdes, A., Gordon, G.W., Algeo, T.J., Boyle, E.A., 2008. Natural fractionation of  $^{238}\text{U}/^{235}\text{U}$ . *Geochimica et Cosmochimica Acta* 72, 345–359.